Phonon branch-resolved electron-phonon coupling and the multitemperature model

Zexi Lu,[1] Ajit Vallabhaneni,[1] Bingyang Cao,[2] and Xiulin Ruan[1,*]

[1]*School of Mechanical Engineering, Purdue University, West Lafayette, Indiana 47907, USA*

[2]*School of Aerospace Engineering, Tsinghua University, Beijing 100084, People's Republic of China*

(Received 25 June 2018; revised manuscript received 7 September 2018; published 17 October 2018)

Electron-phonon (e-p) interaction and transport are important for laser-matter interactions, hot-electron relaxation, and metal-nonmetal interfacial thermal transport. A widely used approach is the two-temperature model (TTM), where e-p coupling is treated with a gray approach with a lumped coupling factor G_{ep} and the assumption that all phonons are in local thermal equilibrium. However, in many applications, different phonon branches can be driven into strong nonequilibrium due to selective e-p coupling, and a TTM analysis can lead to misleading or wrong results. Here, we extend the original TTM into a general multitemperature model (MTM), by using phonon branch-resolved e-p coupling factors and assigning a separate temperature for each phonon branch. The steady-state thermal transport and transient hot electron relaxation processes in constant and pulse laser-irradiated single-layer graphene (SLG) are investigated using our MTM respectively. Results show that different phonon branches are in strong nonequilibrium, with the largest temperature rise being more than six times larger than the smallest one. A comparison with TTM reveals that under steady state, MTM predicts 50% and 80% higher temperature rises for electrons and phonons respectively, due to the "hot phonon bottleneck" effect. Further analysis shows that MTM will increase the predicted thermal conductivity of SLG by 67% and its hot electron relaxation time by 60 times. We expect that our MTM will prove advantageous over TTM and gain use among experimentalists and engineers to predict or explain a wide ranges of processes involving laser-matter interactions.

DOI: 10.1103/PhysRevB.98.134309

I. INTRODUCTION

Electron-phonon (e-p) coupling is an important physical phenomenon that affects Joule heating, laser-matter interaction, and hot electron relaxation [1–8]. A thorough understanding of e-p coupling is crucial for researching material properties as well as advancing the electronic device technology. The two-temperature model (TTM) has been widely used for analysis [9], where electrons and phonons are described as two subsystems with their own temperatures and interact through a coupling factor G_{ep}. Despite the fact that all materials have multiple phonon branches which are different from each other, a simple assumption that all phonons are in thermal equilibrium with a common temperature T_p is used in TTM. It has been combined with multiple methods such as molecular dynamics simulations and proved to be successful in predicting the thermal transport in bulk metal and metal-dielectric interfaces [10–13].

However, recently it has been shown that in certain applications, such as laser heating of semiconductors and metals, phonon branches can be driven into strong nonequilibrium by selective e-p coupling, and an equilibrium picture can result in misleading or wrong interpretations [5]. For example, single-layer graphene (SLG) has drawn intensive attention among researchers as a result of its unique chemical and physical structures [14–18]. Theoretical calculations and experiments such as Raman measurements have been used widely to predict and measure its thermal conductivity [19–26], but the reported values range from 600 to as high as 5800 W/mK [27–31]. Similar with most metals, TTM was used to interpret the experimental measurement and derive k [32]. However, it has been pointed out recently that this method is not accurate since different phonon branches have different coupling strength with the electrons, and their temperatures significantly deviate from each other [5]. As a result, assuming phonon local thermal equilibrium can subsequently underpredict SLG's thermal conductivity by more than 50%. It should be noted that several other mechanisms, such as imperfect experimental conditions and higher order phonon scattering, may also contribute to the uncertainty of graphene thermal conductivity [33–36]. Several other studies on hot electron relaxation in metals or semiconductors also show that the different phonon modes are in nonequilibrium, which can significantly affect the electron cooling rates [37–39]. We can note that the steady-state phonon nonequilibrium within the cooling length region reported in Refs. [5,40] and the transient state phonon nonequilibrium during the phonon relaxation time in Refs. [38,39] are equivalent and due to the same physical origin: modal selective e-p and phonon-phonon (p-p) scattering.

Theoretical methods are needed to capture such modal phonon nonequilibrium. Modal and spatial Boltzmann transport equation (BTE) [41–43] and molecular dynamics combined with modal analysis [44,45] are rigorous and accurate methods, but they are quite complicated and this hinders

*ruan@purdue.edu

their access by experimentalists. Alternatively, a simple multitemperature model (MTM) has been developed which is essentially an extension of TTM that can resolve the temperatures of different phonon branches [5,38]. Subsequently, a detailed proof of such extension was given in Ref. [45] where the relaxation time approximation (RTA) was necessary, suggesting that MTM is rigorously valid when the separated phonon groups couple weakly. For phonon groups that couple strongly, a more rigorous way is to directly treat the scattering. However, the computation cost is high, and we believe in practice we can still use MTM by letting the phonon groups interact with a common thermal reservoir under RTA. This practice has been widely used in the spectral BTE community and the original TTM [9,43,46,47]. Nevertheless, the current MTM models are either still in rather complex forms which hinder easy implementation or only presented in the steady state. Therefore, a simple and explicit approach that can capture the nonequilibrium nature among electrons and phonons is needed to accurately interpret experimental results as well as predicting electronic device performance.

In this study, we will present a general and simple phonon branch-resolved multitemperature numerical simulation approach which can capture the nonequilibrium process between electrons and different phonon branches under both steady and transient states. The original TTM is extended to MTM with e-p coupling strength for each phonon branch. A lattice reservoir which all phonon branches scatter with is defined and the RTA is used. Based on our method, case studies of the steady-state heat transfer and transient hot electron relaxation processes in laser-irradiated SLG are presented respectively. The branch-resolved temperature profiles are shown and the degree of nonequilibrium is discussed. Finally, a comparison with the original TTM is made to show the advantage of MTM.

II. MULTITEMPERATURE MODEL WITH ELECTRON-PHONON COUPLING

The steady-state MTM with e-p coupling has been introduced in our previous work in terms of the e-p cooling power [5]. In this work, we recast it into a more general and convenient form using the e-p coupling factor and extend the original equations to account for the transient heat transfer process as well. The original transient TTM governing equation is

$$\begin{aligned} C_e\frac{\partial T_e}{\partial t} &= \nabla(k_e\nabla T_e) - G_{ep}(T_e - T_p),\\ C_p\frac{\partial T_p}{\partial t} &= \nabla(k_p\nabla T_p) + G_{ep}(T_e - T_p). \end{aligned} \tag{1}$$

Equation (1) describes the two channel-coupled energy transfer process in metals, where their interaction is determined by the coupling factor G_{ep} and their temperature difference. Here e and p refer to electron and phonon respectively. T is the temperature while t is time. k and C refer to the thermal conductivity and volumetric heat capacity of the energy carriers respectively. It can be seen that all the phonons are assumed to be in local thermal equilibrium and assigned to a common temperature T_p. We extend Eq. (1) to account for the phonon branch-resolved temperature and e-p coupling:

$$\begin{aligned} C_e\frac{\partial T_e}{\partial t} &= \nabla(k_e\nabla T_e) - \sum G_{ep,i}(T_e - T_{p,i}),\\ C_{p,i}\frac{\partial T_{p,i}}{\partial t} &= \nabla(k_p\nabla T_p) + G_{ep,i}(T_e - T_{p,i})\\ &\quad + G_{pp,i}(T_{\rm lat} - T_{p,i}), \end{aligned} \tag{2}$$

where i is the index of phonon branches.

Compared with Eq. (1), the e-p coupling term is modified to a branch-resolved form and a p-p coupling term is added for each phonon branch. Here i is the index for phonon branches, and $G_{ep,i}$ is the coupling factor between electrons and phonon branch i. The summation of $G_{ep,i}$ over all the phonon branches will lead to the e-p coupling factor G_{ep} in TTM:

$$\sum G_{ep,i} = G_{ep}. \tag{3}$$

The p-p scattering is represented by the coupling between each phonon branch and the "scattering lattice reservoir" which is represented by an averaged $T_{\rm lat}$. It is an analogy of the e-p coupling using RTA based on the assumption that the p-p scattering has negligible effect on phonon distribution and phase space. $G_{pp,i}$ is the p-p coupling factor between phonon branch i and the scattering lattice reservoir, which is calculated using RTA from the following equation [46–49],

$$G_{pp,i} = \frac{C_{p,i}}{\tau_i}, \tag{4}$$

where τ_i is the relaxation time of phonon branch i and the scattering lattice reservoir's temperature $T_{\rm lat}$ is defined to ensure the energy transfer among phonon branches is conserved:

$$\sum G_{pp,i}(T_{\rm lat} - T_{p,i}) = 0. \tag{5}$$

Then, by solving Eq. (2) numerically, we can obtain the transient and steady-state temperature profiles of the system with resolved electron and phonon branch temperatures. It can be seen that our MTM in Eq. (2) is essentially a spectral treatment of e-p coupling rather than the gray treatment in TTM in Eq. (1). Compared with our previous steady-state MTM [5], in this work we not only extend it to make the transient-state simulation possible but also use the spectral G_{ep} instead of e-p cooling power to describe the phonon branch-resolved coupling strength, which makes our model more general and easier to use.

III. CASE STUDY: THERMAL TRANSPORT IN LASER-IRRADIATED SINGLE-LAYER GRAPHENE

In this section, we will present a case study of the thermal transport process in laser-irradiated SLG. Equation (2) is simplified to its 2D form accordingly.

A. Simulation domain and input parameters

We will use the same input parameter as in Ref. [5]. All of the thermal properties, i.e., the thermal conductivity k, the heat capacity C, the e-p coupling factor G_{ep}, and the p-p coupling factor $G_{pp,i}$ are temperature dependent. Here we

TABLE I. Thermal properties of SLG at 297 K.

Thermal property	LA	TA	ZA	LO	TO	ZO
G_{ep} (10^{16} W/m^{3}K)	0.01	0.0001	0	0.06	0.27	0
G_{pp} (10^{16} W/m^{3}K)	0.27	1.30	0.19	0.27	0.14	0.04
C_p (10^6 J/m^{3}K)	0.19	0.32	0.61	0.03	0.02	0.16
τ (ps)	70.8	24.7	317	10	12	388
k(W/mK)	863.0	237.9	2780.0	10.0	10.0	20.9

report their room-temperature (297 K) values, which are listed in Table I. The details to obtain these values are introduced in Ref. [5] and its supplementary materials. The fact that all the $G_{pp,i}$'s are on the same order with the overall G_{ep} suggests that our previous analogy between e-p and p-p coupling in Eq. (2) is reasonable. The electrons have a heat capacity C_e of 3.6×10^2 J/m^{3}K and a thermal conductivity k_e of 50 W/mK. Our result is higher than the common experimentally measured k_e which is within 10 W/mK, and we attribute this discrepancy to the absence of defects in SLG in our density functional theory calculations. The simulation is conducted on a 10×10 μm SLG, with all four boundaries fixed at 297 K. The system is illustrated in Fig. 1. Initially the entire domain is at a uniform temperature of 297 K, when laser starts to shine at the center of the SLG sample. The expression of the laser spot is as follows:

$$S_{\text{laser}}(r) = 0.063\times10^9\times\exp(-7.744\times10^{16}r^2)\ [\text{W/m}^2], \tag{6}$$

where r (unit: m) is the distance from the center of the sample. The laser energy follows the Gaussian distribution with a laser source of 0.1 mW and a spot radius of 0.5 μm. The electrons are heated up by the laser, which subsequently heat up the phonons. Two cases are investigated on the same system. The first case represents the laser heating process during the Raman experiment where the laser irradiation is constant after the simulation starts. The simulation runs for 50 ns to ensure all temperatures are converged at the steady state. The second case represents a pulse laser heating process which is common in the time-domain thermoreflectance experiments and modern electronics such as the heat-assisted magnetic recording (HAMR) devices [50–53]. A single laser pulse is implemented at the beginning of the simulation with a pulse width of 50 fs, where the laser power is tuned to 100 times larger than the constant irradiation case. Results of the simulations are shown in the next section.

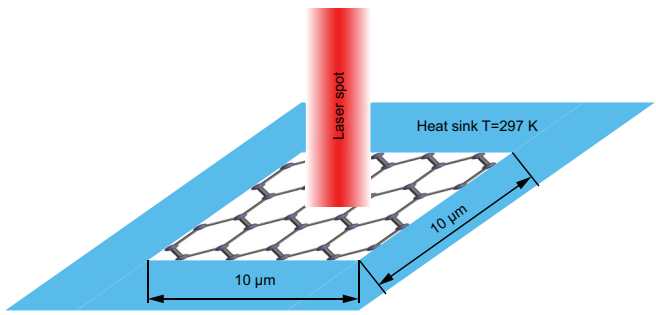

FIG. 1. Illustration of the Raman experiment setup on SLG.

B. Results: Transient and steady-state temperature profile

1. Case A: Constant laser heating

The temperature profile of the center of the SLG for the first 400 ps after the laser is on is shown in Fig. 2(a). Initially the longitudinal optical (LO) and transverse optical (TO) phonons have quicker response to the heating from electrons, while the other phonon branches receive energy much more slowly due to their weak coupling to electrons. The steady-state temperature profile in MTM on SLG, as is shown in Fig. 2(b), is consistent with that reported in our previous work, as expected [5]. In MTM, electrons can reach a temperature of 365 K while the temperature of the scattering lattice reservoir is around 325 K. Electrons and different phonon branches are in significant nonequilibrium. The largest temperature rise on TO phonons is 50 K, which is more than six times larger than the smallest temperature rise of 8 K on out-of-plane acoustic (ZA) phonons, and the cooling radius, which is defined as the distance from the center of the SLG to the position where electrons and phonons reach equilibrium, is 1.5 μm or three times the radius of the laser spot. As expected from the thermal properties in Table I, the LO and TO phonons have higher temperatures. This is because their large G_{ep}'s make them gain energy from electrons efficiently in the center, and their low k also prevents heat from dissipating fast to the boundaries. The ZA branch, on the other hand, is an opposite of these two branches. It cannot receive energy from electrons directly, it only gets heated by the scattering lattice reservoir with a weak coupling factor, and its exceptionally high k helps heat dissipate fast to the boundaries, resulting in a relatively flat temperature profile which stays near the boundary temperature. The longitudinal acoustic (LA), transverse acoustic (TA), and out-of-plane optical (ZO) phonons stay in between as a result of their intermediate thermal properties. It is noteworthy that T_{lat} here is the temperature of the scattering lattice reservoir, which is averaged by G_{pp} over all six phonon branches and does not necessarily represent the apparent lattice temperature that can be observed in experiment. A more detailed discussion will be presented in a later section.

2. Case B: Pulse laser heating

The transient temperature profile of the center of the SLG is shown in Fig. 3(a). During the first 50 fs of the simulation, electrons are heated to a maximum temperature of about 778 K and start to cool sharply after the laser pulse diminishes. The LO and TO phonons undergo similar processes. The other phonon branches, however, still get heated up for a while, as is more clearly shown in Fig. 3(b). Interestingly, electrons become cooler than the TO phonons soon after the laser pulse diminishes. This is because k_e is much higher than k_{LO} while C_e is much smaller than C_{LO}, or the ratio of k/C is much larger for electrons. As a result, electrons dissipate heat more quickly, which leads to an even larger temperature drop, and their temperature profile crosses that of the TO phonons. Similar processes also happen for LA, TA, LO, and ZO phonons, with an exception for the ZA phonons, which have exceptional high thermal conductivity but have no coupling with the electrons. The energy received by ZA phonons from other phonons is dissipated fast to the

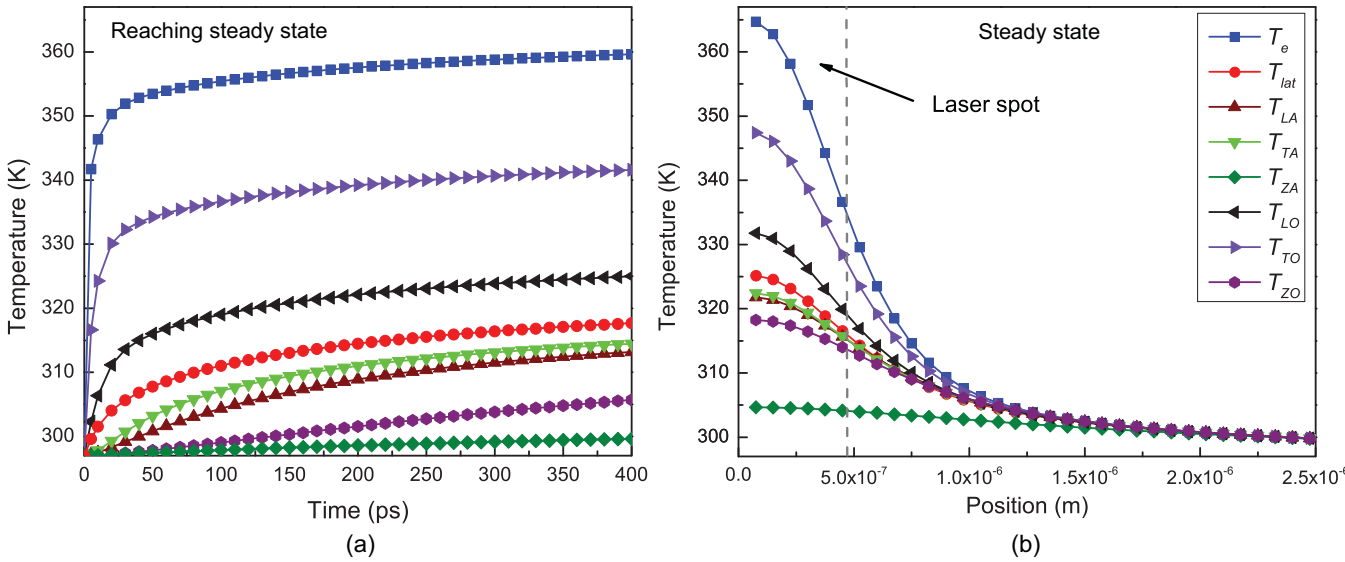

FIG. 2. Temperature profiles of the SLG under constant laser irradiation in MTM: (a) The transient temperature profile in the center of the SLG in the first 400 ps after the laser is on and (b) the steady-state temperature profile of SLG along the line from the center to the midpoint of one boundary.

boundaries and they always stay as the branch with the lowest temperature. Although the temperature difference between different phonon branches and the electrons is smaller than 0.4 K after 120 ps, they are still not in complete equilibrium.

IV. DISCUSSIONS

A. The apparent lattice temperature and degree of nonequilibrium

In the previous section, we have used the scattering lattice reservoir temperature T_{lat} to represent the average phonon temperature. However, questions arise as to whether T_{lat} is the apparent lattice temperature T_p that can be probed in experiments. We argue that the apparent lattice temperature T_p should represent the overall internal energy of the lattice, and hence it should be defined as

$$T_p = \frac{\sum C_{p,i} T_{p,i}}{\sum C_{p,i}}. \tag{7}$$

A plot of the apparent lattice temperature T_p and scattering lattice reservoir temperature T_{lat} is shown in Fig. 4. We can see their deviation is significant inside the laser spot and gradually diminishes as the location approaches the boundaries. This can be explained by the degree of nonequilibrium between different phonon branches. From Eqs. (5) and (7), we can see that T_p is more dominated by the acoustic phonons, especially

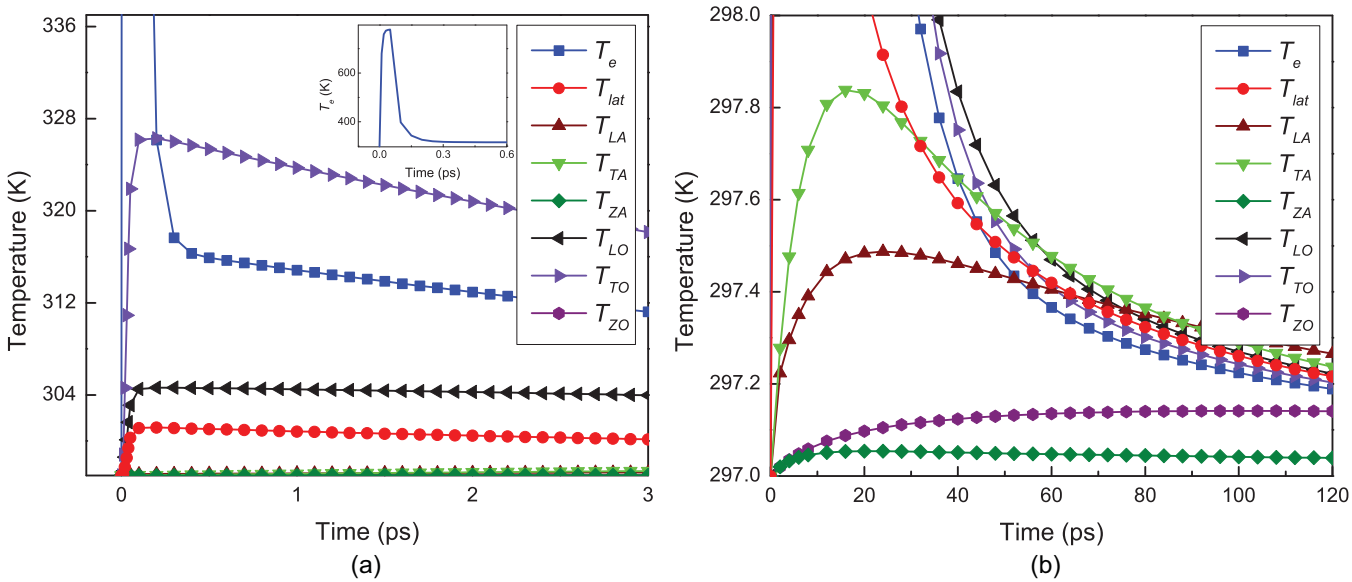

FIG. 3. The transient temperature profiles in the center of the SLG under pulse laser heating in MTM.

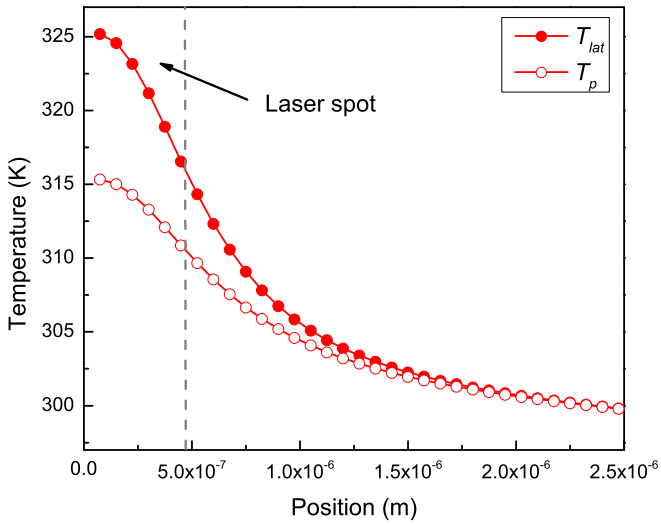

FIG. 4. The comparison between the apparent lattice temperature T_p and the scattering lattice reservoir temperature T_{lat}.

the ZA phonons, because of its large heat capacity, while T_{lat} is more dependent on the branches with higher p-p coupling factor G_{pp}, e.g., the TA phonons. When the phonon branches have great nonequilibrium among each other, e.g., inside the laser spot, the two temperatures deviate from each other. They quickly converge outside the laser spot where the phonon nonequilibrium decreases. Then we plot the normalized deviation of all the six phonon branches, which is defined by

$$\delta = \frac{T_{p,i} - T_p}{T_p - T_0}, \tag{8}$$

where T_0 is the boundary temperature of 297 K. The plot is shown in Fig. 5. The LO, TO, and ZA phonons have the largest deviations, and this is primarily due to their largest and smallest e-p coupling strengths, respectively, as discussed in the previous section. Here we want to propose a simple approximation to estimate their degree of nonequilibrium. As

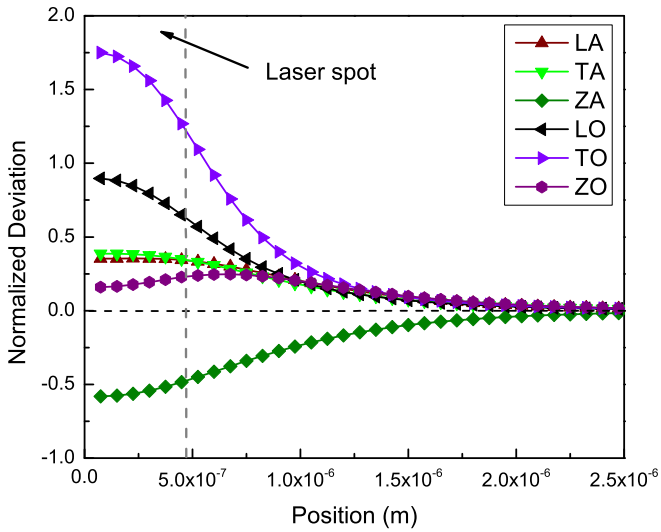

FIG. 5. The normalized deviation of all six phonon branches in SLG.

TABLE II. Ratio of G_{ep}/k and k/G_{ep} of SLG at 297 K.

Thermal property	LA	TA	ZA	LO	TO	ZO
G_{ep}/k	1.0×10^{-3}	1.2×10^{-4}		0.56	2.6	0
k/G_{ep}			∞			

discussed previously, a stronger e-p coupling strength will make the phonon's temperature closer to the electron's, while a larger thermal conductivity will make its temperature profile flatter. For those branches with a higher temperature than T_p, a larger G_{ep} and smaller k will drag its temperature closer to T_e, thus contributing to its deviation from T_p. Therefore, a term G_{ep}/k can be used to determine its degree of nonequilibrium; as this value increases, the more nonequilibrium there will be. Similarly, for those that have lower temperatures than the lattice, the previous term's inverse k/G_{ep} can be used. As this value increases, the more deviation there will be. We tabulate the values of these two terms for each phonon branch of SLG in Table II. It should be noted that a zero value does not necessarily mean the absence of nonequilibrium. The G_{pp} term, on the other hand, will always try to reduce the nonequilibrium.

From the results above, we can gain some insights on how to quickly estimate the degrees of nonequilibrium and assess their significance. For example, during the Raman experiment on SLG, before start one can use the thermal properties of SLG to estimate the degree of nonequilibrium of each phonon branch. The analysis above can provide insights on how accurate the measurement is. Further study can also be oriented since our MTM is not limited only to graphene but can be extended to other materials of higher dimension as well. By performing similar calculations and analysis on other materials, it is also possible to build up a relationship between the G_{ep}/k term and the measured k's error, which can then be used as a simple way to assess experiment accuracy.

B. A comparison with the original two-temperature model

Now with the apparent lattice temperature defined, we present a comparison between our MTM and the conventional TTM. The TTM calculation is conducted on the same system with the same initial and boundary conditions. The thermal properties of the SLG, i.e., k, C, and G_{ep}, are acquired simply by summing up the values used in MTM over all the phonon branches. The heating and steady-state TTM temperature profiles of the system are shown in Fig. 6 along with some representative temperatures from MTM. It can be seen from the figure that MTM and TTM have completely different results. In TTM, the steady-state electron temperature in the center is 340 K while that of phonons is 308 K. The two temperatures quickly get into equilibrium with a cooling radius of approximately 1 μm, or two times the radius of the laser spot. The electron and apparent lattice temperatures in MTM are higher than those in TTM by 50% and 80%, respectively. In addition, in MTM the temperatures of certain phonon branches are significantly higher than the apparent lattice temperature. Interestingly, the TO phonons' temperature in MTM is even higher than the electron temperature in TTM. Due to their strong e-p coupling, the TO phonons get heated up quickly to

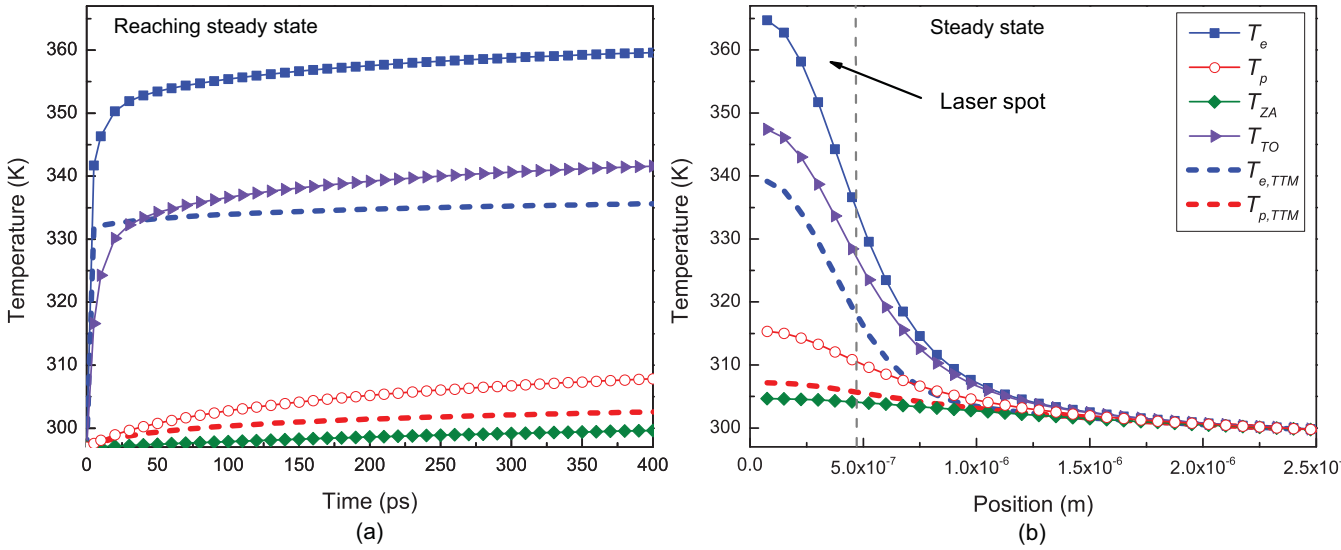

FIG. 6. Temperature profiles of the SLG under constant laser irradiation in TTM: (a) The transient temperature profile in the center of the SLG in the first 400 ps after the laser is on and (b) the steady-state temperature profile of SLG along the line from the center to the midpoint of one boundary. Four representative temperatures from MTM are also included for reference.

a high temperature in MTM. This becomes the so-called hot phonon bottleneck, which in return prevents the electron from cooling and results in a higher electron temperature. Another interesting finding is that the lattice temperature in TTM is very close to the ZA phonons in MTM. This is because in TTM all the phonon branches collapse into one single phonon branch with the combined G_{ep} and k. As a result, the lattice quickly dissipates heat to the boundaries with its large k and stays at a low temperature close to the boundary. The electron temperature is also dragged down, which is even cooler than the TO phonons in MTM. As expected, in TTM the system converges faster to steady state due to the absence of the hot phonon bottleneck.

The large difference between MTM and TTM has important and wide range of implications for processes involving laser-matter interactions. We can regard the MTM temperatures as the "real" temperatures in the experiment. Therefore, in order to increase the temperatures in TTM to match those in MTM, one has to use a smaller k in TTM. Based on Fourier's law of conduction, $k\nabla^2 T + S_{\text{laser}} = 0$, the fitted apparent k will be around 1700 W/mK, less than 60% of the value used in the simulation. Therefore, it is necessary to use MTM instead of TTM for an accurate prediction. In other words, the laser heating leads to an apparent thermal conductivity lower than the intrinsic value as a result of the local thermal nonequilibrium. It also has important implications to thermal

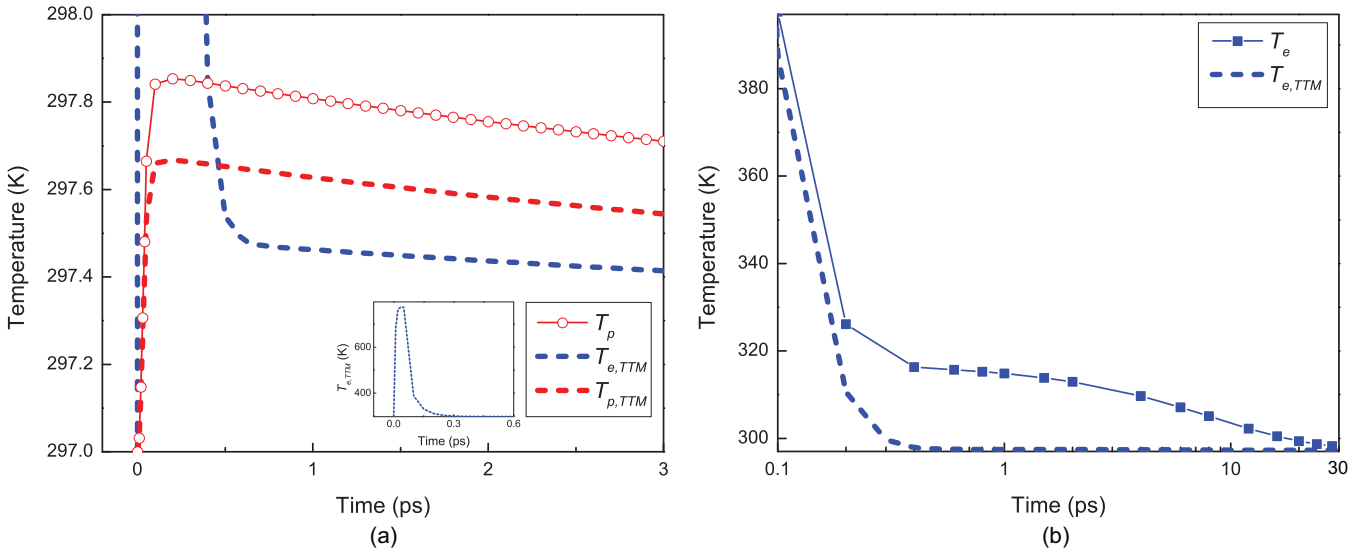

FIG. 7. (a) The transient temperature profiles in the center of the SLG under pulse laser heating in TTM. Figure (b)'s horizontal axis is on logarithmic scale, which shows the electron relaxation in two models.

management of electronic devices. Our MTM shows that certain phonon temperatures can be much higher than the apparent lattice temperature. These hot phonons can displace the lattice along their eigenvectors and result in "nonthermal damage" of the device even though the apparent temperature is still lower than the damage threshold [54,55]. Therefore, MTM is advantageous over TTM for thermal design to better prevent such nonthermal device failures.

We also perform the pulse laser heating simulation using TTM. The transient temperature profile is shown in Fig. 7. Unlike the constant irradiation case, the maximum temperatures of electrons and phonons are almost identical in both models. $T_{e,\mathrm{TTM}}$ has a maximum value of 775 K at 50 fs. The temperature profiles of T_p and $T_{p,\mathrm{TTM}}$ differ by about 30%, but the absolute value is trivial because the lattice heat capacity is much larger than its electronic counterpart and the temperature rise is small. This indicates that using a simple TTM will not affect the prediction of the lattice temperature too much. However, the hot electron relaxation processes are completely different, as is more clearly shown in Fig. 7(b). In TTM, $T_{e,\mathrm{TTM}}$ drops to below 298 K within 0.5 ps, while this only happens to $T_{e,\mathrm{MTM}}$ after more than 30 ps due to the hot optical phonons. Therefore, TTM overpredicts the electron relaxation rate by more than 60 times. Slow electron relaxation is beneficial for solar cells where electron cooling should be minimized for efficiency enhancement [56,57], and hence our MTM will be a much more accurate design tool than TTM.

V. SUMMARY

We have developed a multitemperature simulation approach which can present phonon branch-resolved temperature profile and capture the nonequilibrium thermal transport process. Using temperature-dependent and phonon branch-resolved thermal properties as inputs, we obtained the transient and steady-state temperature profiles of the thermal transport in laser-irradiated SLG. Results show that the phonon branches are in strong nonequilibrium because of their different e-p coupling strengths. The largest temperature rise occurred for the TO phonons is more than six times larger than the smallest of the ZA phonons. The thermal transport is dominated by different material properties during constant and pulse laser heating processes. Then we discuss and define the apparent lattice temperature in MTM and make a comparative study with the original TTM. It is found that TTM predicts a temperature profile significantly lower than MTM, and a simple assumption that ignores the thermal nonequilibrium between phonons can underpredict the thermal conductivity by more than 40%, while overpredicting the hot electron relaxation rate by more than 60 times. We also find that the term G_{ep}/k can be used to estimate the degree of nonequilibrium of phonon branches during a steady-state conduction. We anticipate that our model and results will be useful for experimentalists and engineers in prediction and interpretation of a wide range of processes involving laser-matter interactions. Our model can also be extended to apply to other materials of higher dimensions and eventually become a generalized methodology.

ACKNOWLEDGMENT

The authors are thankful for the support from the National Natural Science Foundation of China (Grant No. 51628602).

[1] P. B. Allen, Phys. Rev. Lett. **59**, 1460 (1987).
[2] D. M. Duffy and A. M. Rutherford, J. Phys.: Condens. Matter **19**, 016207 (2007).
[3] Z. Lin, L. V. Zhigilei, and V. Celli, Phys. Rev. B **77**, 075133 (2008).
[4] J. Zhou, N. Li, and R. Yang, Eur. Phys. J. B **88**, 156 (2015).
[5] A. K. Vallabhaneni, D. Singh, H. Bao, J. Murthy, and X. Ruan, Phys. Rev. B **93**, 125432 (2016).
[6] A. Jain and A. J. H. McGaughey, Phys. Rev. B **93**, 081206 (2016).
[7] F. Giustino, Rev. Mod. Phys. **89**, 015003 (2017).
[8] J. Zhou, H. Zhu, T.-H. Liu, Q. Song, R. He, J. Mao, Z. Liu, W. Ren, B. Liao, D. J. Singh, Z. Ren, and G. Chen, Nat. Commun. **9**, 1721 (2018).
[9] A. Majumdar and P. Reddy, Appl. Phys. Lett. **84**, 4768 (2004).
[10] Y. Wang, X. Ruan, and A. K. Roy, Phys. Rev. B **85**, 205311 (2012).
[11] Y. Wang, Z. Lu, A. K. Roy, and X. Ruan, J. Appl. Phys. **119**, 065103 (2016).
[12] Z. Lu, Y. Wang, and X. Ruan, Phys. Rev. B **93**, 064302 (2016).
[13] Z. Lu, Y. Wang, and X. Ruan, J. Appl. Phys. **123**, 074302 (2018).
[14] E. Pop, V. Varshney, and A. K. Roy, MRS Bull. **37**, 1273 (2012).
[15] Y. Wang, A. K. Vallabhaneni, B. Qiu, and X. Ruan, Nanoscale Microscale Thermophys. Eng. **18**, 155 (2014).
[16] J. Shi, Y. Zhong, T. S. Fisher, and X. Ruan, ACS Appl. Mater. Interfaces **10**, 15226 (2018).
[17] Z.-Y. Ong, B. Qiu, S. Xu, X. Ruan, and E. Pop, J. Appl. Phys. **123**, 115107 (2018).
[18] Y. Wei and R. Yang, Nat. Sci. Rev., nwy067 (2018).
[19] K. M. F. Shahil and A. A. Balandin, Nano Lett. **12**, 861 (2012).
[20] Y. Wang, B. Qiu, and X. Ruan, Appl. Phys. Lett. **101**, 013101 (2012).
[21] W. Park, J. Hu, L. A. Jauregui, X. Ruan, and Y. P. Chen, Appl. Phys. Lett. **104**, 113101 (2014).
[22] X. Shen, Z. Wang, Y. Wu, X. Liu, Y.-B. He, and J.-K. Kim, Nano Lett. **16**, 3585 (2016).
[23] X. Wu, V. Varshney, J. Lee, T. Zhang, J. L. Wohlwend, A. K. Roy, and T. Luo, Nano Lett. **16**, 3925 (2016).
[24] Z. Lin, W. Qin, J. Zeng, W. Chen, P. Cui, J.-H. Cho, Z. Qiao, and Z. Zhang, Nano Lett. **17**, 4013 (2017).
[25] K. Xu, H. Lu, E. W. Kinder, A. Seabaugh, and S. K. Fullerton-Shirey, ACS Nano **11**, 5453 (2017).
[26] J. Shi, J. Lee, Y. Dong, A. Roy, T. S. Fisher, and X. Ruan, Phys. Rev. B **97**, 134309 (2018).
[27] A. A. Balandin, S. Ghosh, W. Bao, I. Calizo, D. Teweldebrhan, F. Miao, and C. N. Lau, Nano Lett. **8**, 902 (2008).

[28] W. Cai, A. L. Moore, Y. Zhu, X. Li, S. Chen, L. Shi, and R. S. Ruoff, Nano Lett. **10**, 1645 (2010).
[29] C. Faugeras, B. Faugeras, M. Orlita, M. Potemski, R. R. Nair, and A. K. Geim, ACS Nano **4**, 1889 (2010).
[30] J.-U. Lee, D. Yoon, H. Kim, S. W. Lee, and H. Cheong, Phys. Rev. B **83**, 081419 (2011).
[31] S. Yiğen and A. R. Champagne, Nano Lett. **14**, 289 (2014).
[32] C. H. Lui, K. F. Mak, J. Shan, and T. F. Heinz, Phys. Rev. Lett. **105**, 127404 (2010).
[33] F. Hao, D. Fang, and Z. Xu, Appl. Phys. Lett. **99**, 041901 (2011).
[34] T. Feng, X. Ruan, Z. Ye, and B. Cao, Phys. Rev. B **91**, 224301 (2015).
[35] H. Malekpour, P. Ramnani, S. Srinivasan, G. Balasubramanian, D. L. Nika, A. Mulchandani, R. K. Lake, and A. A. Balandin, Nanoscale **8**, 14608 (2016).
[36] T. Feng and X. Ruan, Phys. Rev. B **97**, 045202 (2018).
[37] Y. Yang, D. P. Ostrowski, R. M. France, K. Zhu, J. van de Lagemaat, J. M. Luther, and M. C. Beard, Nat. Photon. **10**, 53 (2016).
[38] L. Waldecker, R. Bertoni, R. Ernstorfer, and J. Vorberger, Phys. Rev. X **6**, 021003 (2016).
[39] S. Sadasivam, M. K. Y. Chan, and P. Darancet, Phys. Rev. Lett. **119**, 136602 (2017).
[40] S. Sullivan, A. Vallabhaneni, I. Kholmanov, X. Ruan, J. Murthy, and L. Shi, Nano Lett. **17**, 2049 (2017).
[41] G. Chen, Phys. Rev. B **57**, 14958 (1998).
[42] C. Dames and G. Chen, J. Appl. Phys. **95**, 682 (2004).
[43] D. Singh, J. Murthy, and T. Fisher, in *ASME 2009 InterPACK Conference* (ASME, San Francisco, CA, 2009).
[44] T. Feng, W. Yao, Z. Wang, J. Shi, C. Li, B. Cao, and X. Ruan, Phys. Rev. B **95**, 195202 (2017).
[45] M. An, Q. Song, X. Yu, H. Meng, D. Ma, R. Li, Z. Jin, B. Huang, and N. Yang, Nano Lett. **17**, 5805 (2017).
[46] D. Singh, J. Y. Murthy, and T. S. Fisher, J. Appl. Phys. **110**, 094312 (2011).
[47] D. Singh, J. Y. Murthy, and T. S. Fisher, J. Appl. Phys. **110**, 044317 (2011).
[48] D. J. Sanders and D. Walton, Phys. Rev. B **15**, 1489 (1977).
[49] A. J. H. McGaughey and M. Kaviany, Phys. Rev. B **69**, 094303 (2004).
[50] Y. K. Koh, M.-H. Bae, D. G. Cahill, and E. Pop, Nano Lett. **10**, 4363 (2010).
[51] L. Pan and D. B. Bogy, Nat. Photon. **3**, 189 (2009).
[52] B. Xu, H. Wang, Z. Cen, Z. Liu, K. Ye, H. Yang, J. Zhang, and J. Li, in *2015 IEEE Magnetics Conference (INTERMAG)* (IEEE, Beijing, China, 2015).
[53] J.-A. Yang, S. Parham, D. Dessau, and D. Reznik, Sci. Rep. **7**, 40876 (2017).
[54] Y. Wang and X. Xu, Appl. Phys. A **110**, 617 (2013).
[55] T. Zier, E. S. Zijlstra, A. Kalitsov, I. Theodonis, and M. E. Garcia, Struct. Dyn. **2**, 054101 (2015).
[56] A. J. Nozik, Annu. Rev. Phys. Chem. **52**, 193 (2001).
[57] L. Chen, H. Bao, T. Tan, O. V. Prezhdo, and X. Ruan, J. Phys. Chem. C **115**, 11400 (2011).